Available online at www.sciencedirect.com
ScienceDirect
Journal of Power Sources 163 (2006) 323–329
JOURNAL OF POWER SOURCES
www.elsevier.com/locate/jpowsour

Fabrication and evaluation of Pt–Fe alloys as methanol tolerant cathode materials for direct methanol fuel cells

W. Yuan, K. Scott, H. Cheng *

School of Chemical Engineering & Advanced Materials, University of Newcastle upon Tyne, Newcastle upon Tyne NE1 7RU, England, United Kingdom

Received 1 June 2005; received in revised form 14 August 2006; accepted 12 September 2006
Available online 27 October 2006

Abstract

Carbon-supported platinum–iron catalysts were prepared and characterised by means of scanning electron microscopy, energy-dispersive X-ray and X-ray diffraction techniques. The catalysts were tested for oxygen reduction in half-cells and in direct methanol fuel cells using voltammetric and steady-state polarisation measurements. Methanol oxidation was partially suppressed and higher net oxygen reduction currents were achieved at the PtFe/C cathodes, compared to the Pt alone. An increase in power density of up to 20–30% was achieved by using the PtFe/C rather than the Pt/C cathodes.

Keywords: Platinum–iron alloy; Oxygen reduction reaction; Direct methanol fuel cell; Methanol tolerance

1. Introduction

One of the challenges to commercialise direct methanol fuel cells (DMFC) is to improve poor cathode performance caused by the highly irreversible oxygen reduction reaction (ORR) and negative effect of fuel crossover, leading to a potential loss of 0.1 V and 25% of reduction in efficiency [1–4].

Significant efforts have been made to alleviate or eliminate the negative effect of methanol crossover. One option is to use ruthenium chalcogenide catalysts, e.g. RuSeM (M = Mo, Re, Rh, etc.) and RuSM (M = Rh, Re, Mo, etc.) [5,6]. With these catalysts, the oxidation of methanol on the cathode was greatly suppressed or avoided, and thus the mixed potential was reduced. The main concern for this approach is the rather low power outputs due to low activity of these catalysts for ORR, compared to Pt catalysts. More effort is required to improve their activity.

Another approach is to use carbon-supported macrocycles and their derivatives of Fe or Co, e.g. iron tetramethoxyphenyl porphyrin [7]. The stability of this type of catalyst is a concern especially under acidic conditions, e.g. a fuel cell with an iron tetraphenylporphyrin cathode can be only stable up to 10 h [8].

Pt is the best catalyst we have for the ORR at the moment and great efforts have been made to improve its activity. Low methanol tolerance and high cost of Pt also affect its applications. Alloying Pt with transition metals such as Cr, Fe, Co, Ni, etc. can improve the activity and methanol tolerance of cathodes, reduce catalyst sintering and increase roughness of the catalyst surface and, therefore, improve performance of fuel cells with the Pt alloy cathodes [1,2]. The feasibility of the commercial use of these catalysts is still uncertain. This work was aimed at improving the DMFC performance using PtFe alloy cathodes.

2. Experimental

2.1. Reagents, materials and apparatuses

The chemical reagents and materials with their respective suppliers are: H_2PtCl_6 (99.9%, Janssen), $Fe(NO_3)_3{\cdot}9H_2O$ (AnalaR, BDH), NaOH (AnalaR, BDH), HCl (AnalaR, BDH), H_2SO_4 (AnalaR, BDH), CH_3OH (99.99%, Fisher), carbon powder (Vulcan XC-72R, Cabot), Ketjen-300J carbon black (Akzo Nobel), carbon paper (Toray, TGPH120, E-TEK), PtRu/C (60 wt.% Pt + Ru on Vulcan XC-72R, 1:1 in atomic ratio of Pt to Ru, E-TEK), Nafion® solution (5 wt.%, Aldrich), Nafion® 117 membrane (DuPont), platinum mesh (20 cm^2, 99.99%, Good-

* Corresponding author. Fax: +44 191 222 5292.
E-mail address: hua.cheng@ncl.ac.uk (H. Cheng).

0378-7753/$ – see front matter © 2006 Elsevier B.V. All rights reserved.
doi:10.1016/j.jpowsour.2006.09.005

fellow), and Hg/Hg_2SO_4 (saturated K_2SO_4) reference electrode (MMS, Russell). Deionised water (ELGASTAT B124 Water Purification Unit, the Elga group, England) and high purity gases (hydrogen, nitrogen, air and oxygen, BOC) were used.

2.2. Pt–Fe alloy preparation

Carbon-supported Pt–Fe alloy catalysts with different Pt:Fe atomic ratios were prepared following the impregnation method [9,10]. In a typical run targeting for preparation of 1Pt1Fe/C, 200 mg of Vulcan XC-72R carbon black was dispersed in a 20 ml mixture of *iso*-propanol and deionised water (volume ratio 1:1) at 60 °C under magnetically stirring for 10 min. Then, 100 mg of chloroplatinic acid was added drop wise and stirred for another 10 min. The same procedure was followed to add 94 mg ferric nitrate, $Fe(NO_3)_3{\cdot}9H_2O$. The solution pH was adjusted to 7 using 0.1 mol dm^{-3} hydrazine solution, the final mixture was ultrasonicated for 30 min. The mixture was then filtered and the resultant slurry was transferred into a porcelain boat, which was put in a quartz tube contained in an electric oven and connected tightly to a nitrogen and hydrogen manifold. The sample was alloyed for 1 h (750 °C, 100 ml H_2 min^{-1}) and annealed for 2 h (750 °C, 100 ml N_2 min^{-1}). Three typical Pt:Fe atomic ratios are 3.8:1, 1.2:1 and 1:2.7, which were referred to as 3.8Pt1Fe/C, 1.2Pt1Fe/C and 1Pt2.7Fe/C, respectively.

2.3. Catalyst characterisation

X-ray diffraction (XRD) analysis was carried out with a Siemens D-5005 X-ray Diffractometer using Cu Kα radiation. The tube current is 100 mA and tube voltage is 40 kV. The 2θ angular regions between 20° and 100° were explored at a scan rate of 2° min^{-1}. The Joint Committee of Powder Diffraction Standards was refereed to for peak identification. The lattice parameters of the catalysts were calculated from the broadening X-ray diffraction peak, Pt (1 1 1), using the Scherrer equation [11,12]:

$$L = \frac{K\lambda}{B\cos\theta} \tag{1}$$

where L is the average length of the crystallite, which is proportional to lattice parameters [12], B is the broadening of the line in unit of 2θ and θ is Bragg diffraction angle, K is a constant approximately equal to 0.9 [13] and λ is wavelength. The relative intensity of Pt (1 1 1) crystal face was defined as

$$\Delta I_{1\,1\,1}(\%) = \frac{I_{1\,1\,1}}{\sum I_{h\,k\,l}} \times 100 \tag{2}$$

where $\sum I_{h\,k\,l}$ was calculated based on four main diffraction peaks, Pt (1 1 1), Pt (2 0 0), Pt (2 2 0) and Pt (3 1 1).

Scanning electron microscopy (SEM) and energy-dispersive X-ray (EDX) measurements were carried out using a JEOL JSM-5300LV scanning electron microscope at an acceleration voltage of 25 kV and a ROUTEC UHV Dewar Detector.

2.4. Half-cell test

An undivided three-electrode glass cell (200 cm^3 in volume) was used for most half-cell measurements. Circular working gas diffusion electrodes with a loading of 1 mg Pt cm^{-2} were prepared by pasting a mixture of the catalyst and Nafion® (30% of loading using 5 wt.% Nafion® solution) in *iso*-propanol onto carbon paper. After hot-pressing at 100 kg cm^{-2} and 130 °C, the electrodes were mounted in the cell, in which the electrode holder was designed such that gasses can be passed at the rear-side of the electrode and penetrated into solution via the front face of the electrode. A platinum mesh (20 cm^2) and an MMS were used as the counter and reference electrodes, respectively.

Cyclic voltammetry and steady-state galvanostatic polarisation were performed using the Sycopel Potentiostat system consisting of a 10 A–20 V Potentiostat and a PCI-100 signal generator (Scientific Limited, England). A gas flow rate of 25 cm^3 min^{-1} was used to fresh working solutions in each run. All new electrodes were treated by cycling between 0.3 and −1.0 V versus MMS for 50 cycles at a scan rate of 50 mV s^{-1}, which made the surface wet and reproducible. The steady-state measurements were achieved by holding the cathode potential at open circuit potential for 1 min, and then stepping to −0.4 V versus MMS for about 3 min.

To characterise the effect of methanol on the ORR, a methanol effect coefficient (χ) was defined:

$$\chi = \frac{j_0 - j_{\text{methanol}}}{j_0} \tag{3}$$

where j_0 and j_{methanol} are absolute values of net current densities at a fixed potential (mA cm^{-2}) in blank and methanol solutions, respectively, i.e.:

$$j_0 = (j_{O_2} - j_{N_2})_{\text{blank}} \tag{4}$$

$$j_{\text{methanol}} = (j_{O_2} - j_{N_2})_{\text{methanol}} \tag{5}$$

where j_{O_2} and j_{N_2} are absolute values of current densities in solutions saturated with oxygen and nitrogen, respectively.

The electrochemical active surface areas of the PtFe electrodes were calculated based on the coulomb charge, assuming a value of 210 μC cm^{-2} for the charge related to hydrogen adsorption on a smooth Pt surface [14]. The amounts of charge were determined as the mean value between the amounts of charge exchanged during the electro-adsorption and desorption of atomic hydrogen on the Pt sites from the relevant regions of the CVs, taking into account the correction for double-layer charging in the region [14,15].

2.5. Fuel cell test

All membrane electrode assemblies (MEAs) were fabricated under comparable conditions, e.g. using the same catalyst loading (1 mg Pt cm^{-2} + 0.52 mg Ru cm^{-2} for anodes and 1.0 mg Pt cm^{-2} for cathodes and Nafion® 117 membrane). Ketjen-300J carbon black (1 mg C cm^{-2}) was always used in the gas diffusion layer after mixed with 20 wt.% Teflon and *iso*-propanol and thus obtained catalyst suspension was deposited

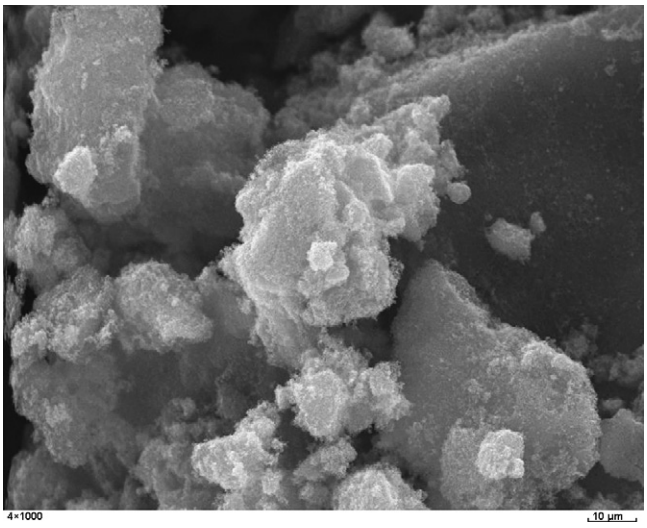

Fig. 1. Scanning electron micrograph of the 1Pt2.7Fe/C material (1000×).

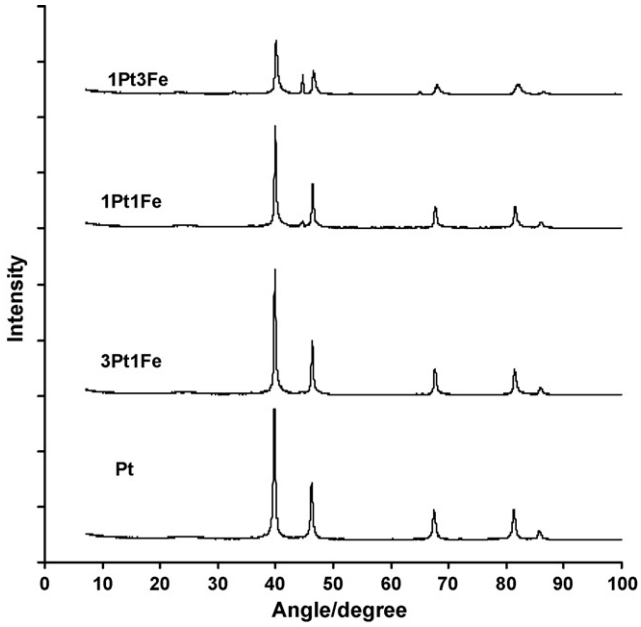

Fig. 2. Powder XRD patterns of the PtFe/C materials.

onto the carbon paper support layer by layer (ca. 0.5 ml for each layer) using a pipette. The suspension was spread uniformly over the entire surface with the pipette tip. A hairdresser was used to accelerate the drying of the catalysts suspension between each application. Nafion® ionomer (10 wt.%) and *n*-butyl acetate or *iso*-propanol was used to prepare the inks for the catalytic layers of the anode and cathode, respectively. Finally, a thin layer of Nafion® solution (1 mg Nafion cm^{-2}) was spread onto the surface of each electrode and allowed them dry under atmospheric conditions. MEA was obtained by pressing the anode and cathode on either side of the Nafion® 117 membrane under a pressure of 50 kg cm^{-2} at 130 °C for 3 min.

Details in assembling and operation of DMFCs were described elsewhere except for the different active area (4 cm^2) [16]. For measurements of polarisation curves for individual electrodes in situ of the DMFC, hydrogen gas was purged into the cathode chamber, which formed a combined counter and reference electrode [17,18].

3. Results and discussion

3.1. Structural characteristics

Fig. 1 shows typical SEM picture for the 1Pt2.7Fe/C material, where the catalyst surface appears highly porous consisting of cauliflower-like clusters. The chemical compositions of three PtFe/C catalysts determined by EDX are shown in Table 1. Different Pt:Fe ratios were obtained by controlling amounts of Pt and Fe salts during the preparation.

Fig. 2 shows representative X-ray diffraction patterns for the PtFe/C and the Pt/C materials. The main diffraction peaks observed in the spectra can be identified as the crystal faces Pt (1 1 1), Pt (2 0 0), Pt (2 2 0) and Pt (3 1 1) with slightly changed 2θ positions. The Pt (1 1 1) peak 2θ positions, the lattice parameter and the relative intensity of the Pt (1 1 1) peak are listed in Table 1. The lattice parameter decreased and the relative intensity of Pt (1 1 1) crystal face increased with increasing Fe content. All three samples exhibited only a face-centred cubic structure with the lattice parameters of 0.3815–0.3835 nm. The values are smaller than that of the Pt/C, i.e. 0.3928 nm, because the Fe metal entered into the crystal structure of Pt and the crystal axis shortened [19]. Monotonous shifts of diffraction peaks between those of pure Pt and Fe (not shown here) were observed, which is evidence of the formation of PtFe alloys with solid solution phases or disordered crystallite structure, as reported previously [9]. The peak corresponding to crystal face Fe (1 1 0) (at $2\theta \approx 45.3°$) was not fully developed for the 3.8Pt1Fe sample, but appeared

Table 1
EDX, XRD and CV analyses of the PtFe/C catalysts

Sample	EDX data (at.%)			XRD data			CV data
	C	Pt	Fe	2θ[a] (°)	$I_{111}/\sum I_{hkl}$ (%)	L[b] (nm)	S[c] (cm^2)
1Pt2.7Fe	89.43	2.86	7.71	40.08	59.1	0.3815	324.5
1.2Pt1Fe	95.75	2.35	1.91	39.97	58.7	0.3828	321.8
3.8Pt1Fe	95.28	3.74	0.98	39.91	58.2	0.3835	314.6
Pt				39.81	55.2	0.3928	242.5

[a] Pt(1 1 1) crystal face.
[b] The lattice parameters, which were calculated using (1 1 1) crystal face of Pt.
[c] Electrochemical active surface area.

Table 2
Data from the half-cell measurements[a]

Cathodes	j_0[b] (mA cm^{-2})	$j_{methanol}$[c] (mA cm^{-2})			χ[d] (%)		
		0.1	0.5	1	0.1	0.5	1
Pt	76.8	65.0	62.4	60.2	15.4	18.8	21.6
3.8Pt1Fe	80.3	75.5	67.3	65.2	6.0	16.2	18.8
1.2Pt1Fe	81.2	76.8	68.5	66.4	5.4	15.6	18.2
1Pt2.7Fe	82.9	78.6	70.2	68.1	5.2	15.3	17.9

[a] The data were collected at −0.4 V at 3 min and average values from two or three measurements were included in the table. The conditions are same as those in Fig. 3 except for different cathodes with the same Pt loading (1 mg Pt cm^2).
[b] Net current density collected in the solution saturated with O_2 without methanol.
[c] Net current density collected in the solution saturated with O_2 in the presence of 0.1, 0.5 and 1 mol dm^{-3} methanol.
[d] Methanol oxidation effect coefficient collected in the solution saturated with O_2 in the presence of 0.1, 0.5 and 1 mol dm^{-3} methanol.

at 1.2Pt1Fe and 1Pt2.7Fe samples. The Fe phase of the 1Pt2.7Fe sample showed an additional peak for Fe (2 0 0), at $2\theta = 65.9°$.

The electrochemical active surface area for the alloys and the Pt/C, calculated from the coulomb charge in the region of the hydrogen adsorption and desorption of the cyclic voltammograms (not shown here to remain concise), are summarised in Table 1. All alloys displayed higher active area than the Pt, mainly due to the absorption of the H_2 on Fe and Fe alloys.

3.2. Test of the PtFe/C in half-cell

Fig. 3 shows the half-cell performance of the 1Pt2.7Fe/C and the Pt/C gas diffusion electrodes in 0.5 mol dm^{-3} sulphuric acid solution, with or without methanol, where current density is normalised to the Pt loading. The two electrodes showed similar cyclic voltammograms for ORR in methanol-free solutions (only that of the 1Pt2.7Fe/C is shown here for clarity) with a smooth start and end, but rapidly increased reduction currents, indicating the high activity of these electrodes. In 1 mol dm^{-3} methanol solution, methanol was oxidised on the both electrodes

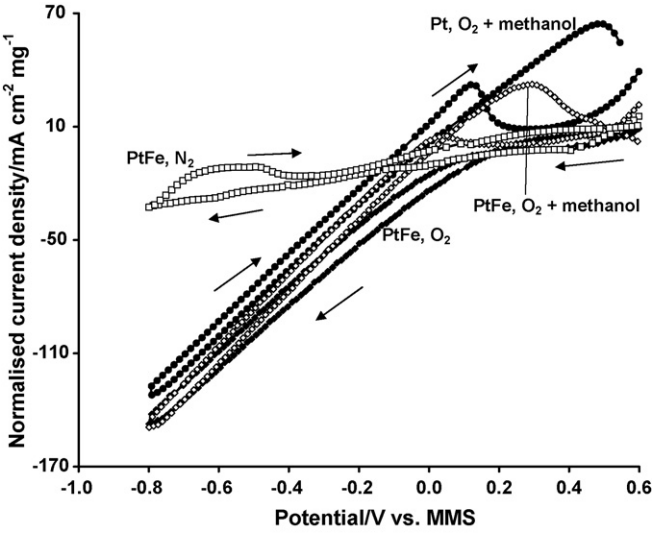

Fig. 3. Cyclic voltammograms on the 1Pt2.7Fe/C and Pt/C gas diffusion electrodes in 0.5 mol dm^{-3} H_2SO_4 solution saturated with O_2 or N_2 with or without 1 mol dm^{-3} CH_3OH. Cell: undivided glass cell; counter electrode: Pt mesh (20 cm^2); scan rate: 50 mV s^{-1}; gas flow rate: 25 cm^3 min^{-1}; temperature: 18 ± 0.5 °C. The arrows indicate scan directions.

during the initial scan and the oxidation currents decreased gradually until a sharp or broad peak for the methanol oxidation with the peak current density of 32.2 and 6.9 mA cm^{-2} for the Pt/C or 1Pt2.7Fe/C electrode, respectively, suggesting higher methanol tolerance of the latter. Current densities for the ORR in 1 mol dm^{-3} methanol solution was higher at the 1Pt2.7Fe/C than at the Pt/C, but lower than those observed in the methanol-free solutions, due to the negative effect of methanol on ORR at these electrodes. Similar behaviour was observed during the reverse scan. These observations mean that alloying Pt with Fe could alleviate the negative effect of methanol oxidation on the ORR.

The steady-state polarisation data are presented in Table 2 and all the PtFe/C catalysts showed better methanol tolerance than the Pt/C as evidenced by a higher current density at a fixed potential and lower methanol oxidation effect coefficients. For example, the net reduction current densities were 78.6 and 65.0 mA cm^{-2} and the methanol oxidation effect coefficients were 5.2 and 15.1% in the 0.1 mol dm^{-3} methanol solution for the 1Pt2.7Fe/C and the Pt/C electrodes, respectively.

As is well known, iron itself is not an active site for ORR [9], but alloying it with Pt can lead to performance enhancement due to several effects, such as:

(i) *Structural effect*. As shown in Table 2, lattice parameter decreased because Fe entered into the crystal structure of Pt and shorted the crystal axis during the alloy process [19]. Such lattice contractions resulted in a more favourable Pt–Pt distance for weakening Pt–oxygen bond and facilitating the dissociative adsorption of O_2 [9,20]. As mentioned above, active surface area of the PtFe/C alloys was larger than that of Pt/C, which was also contributed to increased activity of the alloys for ORR. On the other hand, the ORR was sensitive to the Pt surface structure [21] and the Pt atoms on the Pt (1 1 1) crystal face were more active than those on Pt (2 0 0), Pt (2 2 0) and Pt (3 1 1) faces for ORR due to lateral adsorption of oxygen atoms and enhanced activity for H_2O_2 decomposition, which led to the four-electron reduction process [13,22]. Our XRD measurements showed that the relative content of the Pt (1 1 1) crystal face in three PtFe/C catalysts is higher than that in the Pt/C catalyst (Table 2), which may play roles in their higher activity for ORR, although the XRD does not guar-

antee that the "surface" of PtFe particle has a well-defined (1 1 1) structure. A further investigation is needed to understand the effect.

(ii) *Electronic effect*. Replacement of O–Pt by O–Fe interactions caused change in electronic structure. Fe has more 5d vacancies than Pt so there are more 5d vacancies on the PtFe alloy surface, compared to Pt alone, which caused an increase in 2π electron donation from O_2 to the surface of Pt. Also, O–Fe bond (2.0 Å) is shorter and thus, stronger than O–Pt bond (2.5 Å) [23]. The formation of O–Fe bonds shifted the adsorption energies in favour of the interaction between the oxygen atom and the PtFe alloy surface. Consequently, resulting in an increased adsorption between the Pt and O_2 was enhanced and the O–O bond was weakened [24,25] as well as created more surface sites for adsorption of O_2 on the Pt surface in the alloys than on Pt/C electrocatalyst [24]. The adsorption strength of hydrogen species was also affected by alloying because Pt became more electropositive upon alloying. The changed electronic environment severely limited the adsorption of protons since the adsorption strength of hydrogen is much weaker than that of oxygen at the Pt surface. These factors caused higher catalytic activity of the alloys [9]. When the content of the Fe became too large, e.g. above 50 at.%, the resulting large d vacancy may contribute just to the enhancement of the Pt–O bonding and O–O bond scission or to restrained a reaction beyond the surface oxide formation, resulting in the lowered ORR rate, similar as OH_{ads} impeded the ORR on a single-crystal Pt [26]. Also, at high Fe contents, the Fe particles may constitute a barrier to the free diffusion of oxygen to the active sites, thereby lowering the activity of the catalysts. This explains lower activity of 1Pt3.8Fe/C, compared to other PtFe alloys.

(iii) *Chemical effects*. PtFe alloy showed the higher peroxide decomposition activity due to the role of the dissolved Fe during DMFC operation [13].

The above effects were interplayed and resulted in an enhancement of oxygen-containing species from the electrolyte onto Pt or Fe, particularly, affected the strength of the $[Pt–HO_2]_{ads}$, the key intermediate during ORR, therefore, higher activity for ORR was observed on the PtFe alloy than on Pt [27].

The better methanol tolerance of the PtFe alloys than Pt can be attributed to the role of the Fe addition. Iron itself is not active for methanol oxidation and its addition will partly block contact between Pt particles and methanol molecules, which suppresses methanol oxidation on the binary-component catalyst because the dissociative chemisorptions of methanol requires the existence of several adjacent Pt ensembles [25,28]. More importantly, as shown in the quantum calculations, Pt has a strong tendency to react with organic compounds, but alloying with Fe strongly depresses the interaction energy values and the affinity of PtFe catalysts towards organic compounds and thus, results in higher methanol tolerance than Pt [29,30].

The measurements in half-cell provided useful data to evaluate activity and methanol tolerance of the materials. However, conditions used in a half-cell were far from those experienced in fuel cell. So test of PtFe/C cathode materials were carried out in fuel cells in order to thoroughly check their activity, methanol tolerance and stability.

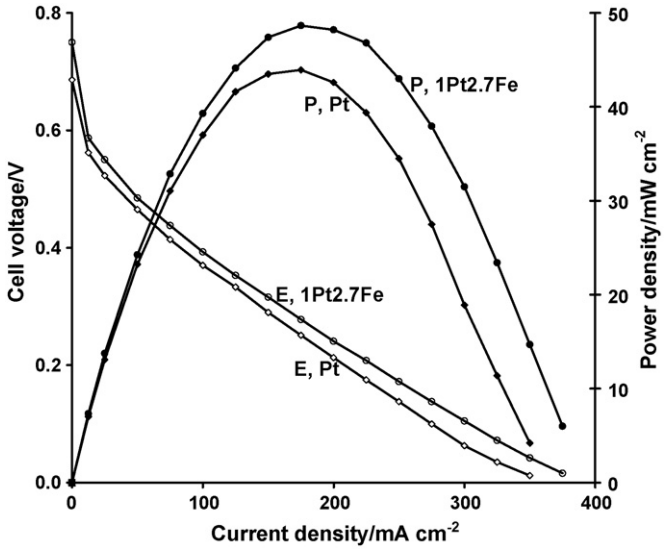

Fig. 4. Steady-state cell voltage (E) and power density (P) vs. current density curves for the DMFCs with the 1Pt2.7Fe/C and Pt/C cathodes. Active area of the cell: 4 cm^2; anode: PtRu/C (1 mg PtRu cm^{-2}, i.e. 1 mg Pt cm^{-2}); cathode loading: 1.0 mg Pt cm^{-2}; membrane: Nafion® 117; fuel: 1 mol dm^{-3} methanol (10 cm^3 min^{-1}); oxidant: O_2 (ambient pressure, 200 cm^3 min^{-1}); temperature: 90 °C.

3.3. Test of PtFe/C cathodes in DMFCs

Fig. 4 shows that there is a better performance of the MEAs with the PtFe alloy cathodes than that with the Pt/C cathode, i.e. 20–30% higher in terms of power density. The better performance of the PtFe/C catalysts, compared to the Pt/C cathode, can be attributed to the enhanced activity for ORR and the better methanol tolerance, in agreement with the half-cell results.

The cathode behaviour had a greater effect on the cell behaviour than that of the anode, as indicated in Fig. 5, where polarisation curves for individual electrodes and the complete cell, measured in situ of the DMFC with the 1Pt2.7Fe/C cathode are shown. Deterioration in DMFC performance was dominated by both cathode and anode polarisation losses, suggesting that a further improvement in electrode performance is required.

Fig. 6 shows the effect of increasing methanol concentration and temperature on the MEAs with the PtFe/C and Pt/C cathodes. In the case of Pt/C, much higher performance loss was observed, e.g. 0.692–0.562 V in the OCV and 43.9–22.6 mW cm^{-2} in peak power density, with an increase in methanol concentration from 1 to 4 mol dm^{-3}. This means that methanol crossover losses counteracted any potential benefit effect of increasing methanol concentration on the anode performance. In the case of 1Pt2.7Fe, losses were relatively smaller, e.g. 0.715–0.590 V and 48.7–33.2 mW cm^{-2}. These data highlight the beneficial effect of operating the DMFC with a PtFe/C catalyst.

As expected, operating the cell with O_2 rather than air, provided better performance (Fig. 7) due to the lower partial

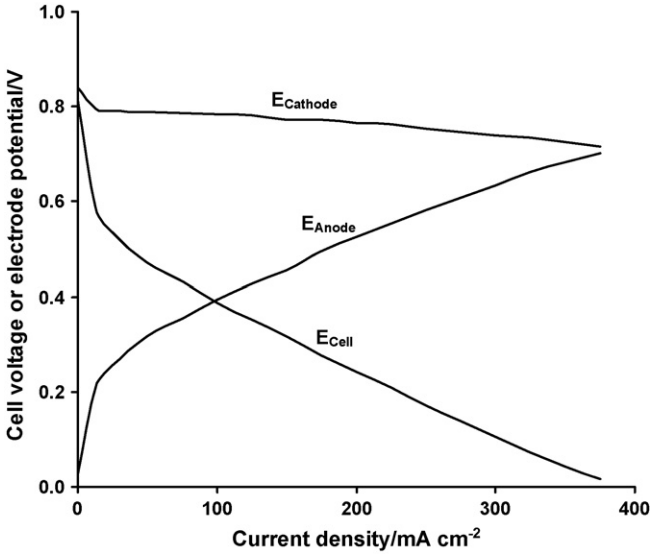

Fig. 5. Steady-state cell and electrode polarisation curves for the DMFC with the 1Pt2.7Fe/C cathode. Conditions as in Fig. 4.

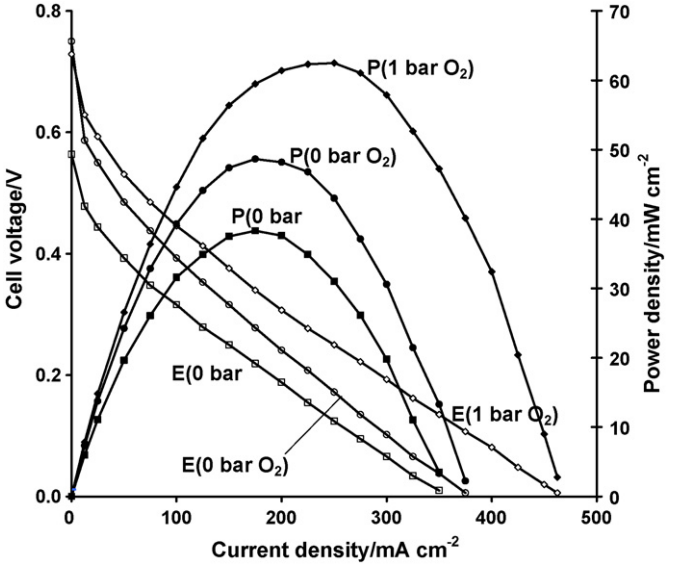

Fig. 7. Steady-state cell voltage (E) and power density (P) vs. current density curves for the DMFC with the 1Pt2.7Fe/C cathode under different oxidant conditions. Other conditions as in Fig. 4.

pressure of oxygen in air and the diffusive blanketing effect of nitrogen in air [31]. An increase in gas pressure increases both the reversible potential of the FC reactions and the exchange current density of the ORR, due to an increase in the gas solubility. Raising the pressure to 1 bar O_2 led to an increase in peak power density from 38.3 to 50.6 and 48.7 to 68.5 mW cm^{-2} for air and O_2, respectively, in the cell with the 1Pt2.7Fe/C cathode. Pressurisation also allowed for much lower oxidant flow rates, e.g. <0.001 dm^3 min^{-1}. The OCV was significantly affected by pressure, e.g. a 30 mV increase in OCV corresponding to a 1 bar increase in O_2 pressure, due to the counteracting effect on methanol crossover.

One concern regarding PtFe alloys is their stability and Fig. 8 shows data collecting in a 60 h period (the values varied when the fresh solution was added or restarted the operation after the interruption). Before the durability test, the MEAs were used for over 300 h under various conditions including conditioning, measurements and maintenance. A decrease of 25 and 75 mV in cell voltage were observed during the period for the MEAs with the 1Pt2.7Fe and Pt cathodes, respectively, corresponding to a power density loss of 1.25 and 3.75 mW cm^{-2}. The data suggested that the 1Pt2.7Fe cathode was more stable than the Pt cathode. This is not surprised because the dissolved Fe and Fe could act as a redox couples and formed complexes with the intermediates, e.g. H_2O_2, which was further reduced by Pt to release H_2O [13,32]. As indicated before, the PtFe alloys exhibit contractions in their Pt–Pt distances, in addition to the formation

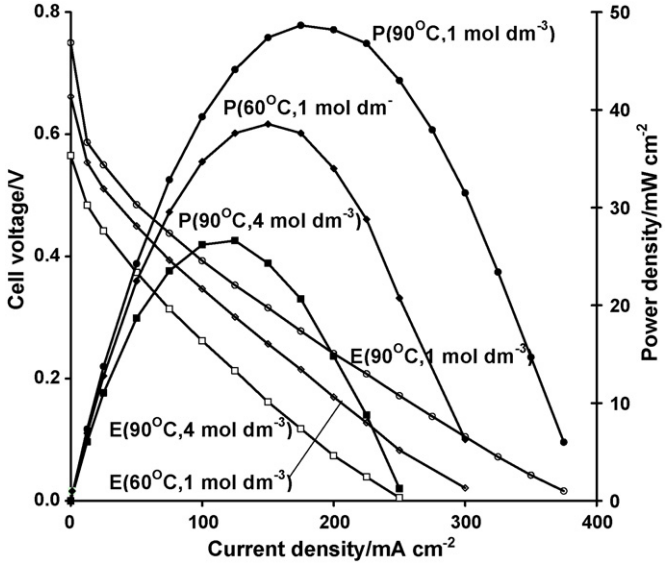

Fig. 6. Steady-state cell voltage (E) and power density (P) vs. current density curves for the DMFC with the 1Pt2.7Fe/C cathode under different conditions (methanol concentration and temperature). Other conditions as in Fig. 4.

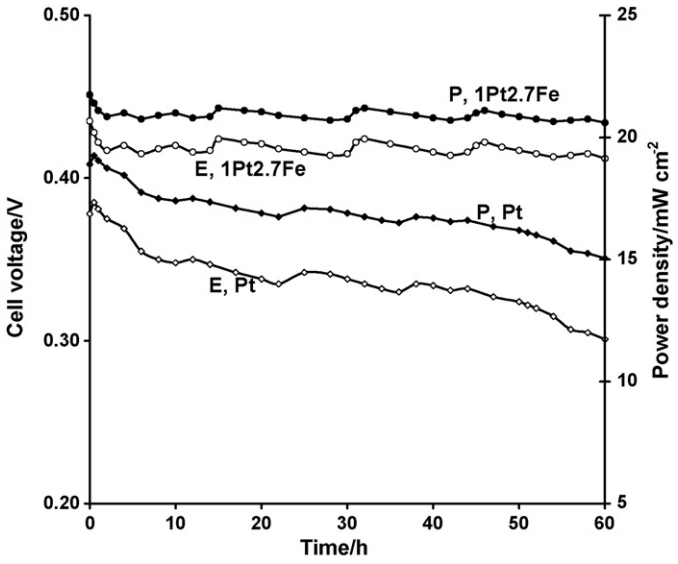

Fig. 8. Cell voltage change with working time for the DMFCs with the 1Pt2.7Fe/C and the Pt/C cathodes at 50 mA cm^{-2} and 60 °C. Other conditions as in Fig. 4.

of very strong O–Fe bonds, changed the segregation profile of the PtFe alloy surface via reorder or reconstruction processes and resulted in a more stable configuration that resists reconstruction at negative potentials and renders the electrocatalysts immune to structural changes in the hydrogen region [25,33]. On the other hand, as well known, Fe has a strong tendency to alloy with carbon, therefore, the Pt atoms are bonded more strongly to the carbon substrate through bridges of Fe atoms, which inhibited the agglomeration and leaching of Pt catalysts during operation, leading to higher stability of the PtFe alloys relative to Pt alone catalysts [10,34]. A slight decrease in performance was due to chemical and thermal deactivations occurred during the operation.

Overall, the data showed that the cell performance of MEAs with the PtFe/C cathodes was clearly better than with Pt/C based MEA. The PtFe catalysts had higher activity for ORR, which partially originated from the difference of active surface area, and better methanol tolerance than the Pt catalyst, which confirmed the trends of the half-cell tests.

4. Conclusions

The three PtFe/C alloys with different compositions have been fabricated and used as cathodes in the DMFCs. The alloying of Pt with Fe suppressed methanol oxidation on the alloy cathode, leading to higher activity for ORR and better methanol tolerance than Pt. Consequently, all alloys showed better performance than the Pt alone, e.g. 20–30% increases in power density. The improvements resulted from the modification of the structural, electronic and chemical properties of Pt with the presence of Fe.

For all alloys tested, increasing the methanol concentration decreased the performance, which could be from a higher methanol crossover rate and its effect on the cathode function. Cell temperature appeared to significantly affect the OCVs by enhancing methanol crossover as the temperature increased. At higher current densities, the performance increased with increasing temperature due to the enhanced reaction kinetics and higher mass transfer coefficients of the reactants. Higher back pressure was beneficial to the performance due to the counteracting effect on the methanol crossover and the increased oxidant supply. The alloying of Pt with Fe improved the cathode stability.

Acknowledgements

The authors thank the Carbon Trust and EPSRC for funding. The work was performed in research facilities provided through an EPSRC/HEFCE Joint Infrastructure Fund award (No. JIF4NESCEQ).

References

[1] H. Yang, N. Alonso-Vante, C. Lamy, D.L. Akins, J. Electrochem. Soc. 152 (2005) A704.
[2] L. Xiong, A. Manthiram, J. Electrochem. Soc. 152 (2005) A697.
[3] A.S. Arico, S. Srinivasan, V. Antonucci, Fuel Cells 1 (2001) 133.
[4] X. Ren, P. Zelenay, S. Thomas, J. Davey, S. Gottesfeld, J. Power Sources 86 (2000) 111.
[5] R.W. Reeve, P.A. Christensen, A.J. Dickinson, A. Hamnett, K. Scott, Electrochim. Acta 45 (2000) 4237.
[6] T.J. Schmidt, U.A. Paulus, H.A. Gasteiger, N. Alonso-Vante, R.J. Behm, J. Electrochem. Soc. 147 (2000) 2620.
[7] P. Convert, C. Coutanceau, F. Claguen, C. Lamy, J. Appl. Electrochem. 31 (2001) 945.
[8] M. Lefevre, J.P. Dodelet, Electrochim. Acta 48 (2003) 2749.
[9] J.T. Hwang, J.S. Chung, Electrochem. Acta 38 (1993) 2715.
[10] Z. Wei, H. Guo, Z. Tang, J. Power Sources 62 (1996) 233.
[11] R.L. Snyder, in: E. Lifshin (Ed.), X-ray Characterization of Materials, Wiley–VCH, Weinheim, 1999, pp. 1–103.
[12] L.V. Azaroff, M.J. Buerger, The Powder Method in X-ray Crystallography, Mcgraw-Hill Book Company, New York, 1958.
[13] W. Li, W. Zhou, H. Li, Z. Zhou, B. Zhou, G. Sun, Q. Xin, Electrochem. Acta 49 (2004) 1045.
[14] A. Pozio, M. De Francesco, A. Cemmi, F. Cardellini, L. Giorgi, J. Power Sources 105 (2002) 13.
[15] O. Antoine, Y. Bulte, P. Ozil, R. Durand, Electrochem. Acta 45 (2000) 4493.
[16] H. Cheng, K. Scott, J. Power Sources 123 (2003) 137.
[17] M.M. Mench, H.M. Chance, C.Y. Wang, J. Electrochem. Soc. 151 (2004) A144.
[18] S.-J. Shin, J.-K. Lee, S.-Y. Ha, S.-A. Hong, H.-S. Chun, I.-H. Oh, J. Power Sources 106 (2002) 146.
[19] W.H. Lizcano-Valbuena, V.A. Paganin, C.A.P. Leite, F. Galembeck, E.R. Gonzalez, Electrochem. Acta 48 (2003) 3869.
[20] J.M. Tian, F.B. Wang, Z.H.Q. Shan, R.J. Wang, J.Y. Zhang, J. Appl. Electrochem. 34 (2004) 461.
[21] C. Rice, Y. Tong, E. Oldfield, A. Wieckowski, Electrochem. Acta 43 (1998) 2825.
[22] S. Srinivasan, O.A. Velev, A. Parthasarathy, D.J. Manko, A.J. Appleby, J. Power Sources 36 (1991) 299.
[23] A.J. Appleby, Energy 11 (1986) 13.
[24] R. Hirsch, F. Delbecq, P. Sautet, J. Hafner, J. Power Sources 217 (2003) 354.
[25] G.Q. Sun, J.T. Wang, R.F. Savinell, J. Appl. Electrochem. 28 (1998) 1087.
[26] J. Shim, D.-Y. Yoo, J.-S. Lee, Electrochem. Acta 45 (2000) 1943.
[27] S. Mukerjee, S. Srinivasan, M.P. Soriaga, J. McBreen, J. Electrochem. Soc. 142 (1995) 1409.
[28] N.M. Markovic, P.N. Ross, Surf. Sci. Rep. 45 (2002) 121.
[29] A. Fortunelli, A.M. Velasco, J. Mol. Struct.: Theochem 586 (2002) 17.
[30] A. Fortunelli, A.M. Velasco, J. Mol. Struct.: Theochem 528 (2000) 1.
[31] L.R. Jordan, A.K. Shukla, T. Behrsing, N.R. Avery, B.C. Muddle, M. Forsyth, J. Power Sources 86 (2000) 250.
[32] Z. Sun, H.C. Chiu, A.C.C. Tseung, Electrochem. Solid-State Lett. 4 (2001) E9.
[33] S. Mukerjee, J. McBreen, J. Electrochem. Soc. 143 (1996) 2285.
[34] Z.D. Wei, F. Yin, L.L. Li, X.W. Wei, X.A. Liu, J. Electroanal. Chem. 541 (2003) 185.